ATLAS PUB Note
ATL-PHYS-PUB-2017-014
July 20, 2017

Performance of the reconstruction of large impact parameter tracks in the inner detector of ATLAS

The ATLAS Collaboration

The standard ATLAS track reconstruction is designed for primary charged particles, which are promptly produced from *pp* collisions. Strict requirements on the transverse and the longitudinal impact parameters are applied to increase the purity of primary charged particle reconstruction while keeping the reconstruction efficiency high and the computation time affordable. A side effect of these criteria is a low efficiency for reconstructing secondary particles originating a significant distance from the interaction point. The addition of a second pass of track reconstruction using left-over hits, and re-optimized requirements on the transverse and longitudinal impact parameters, significantly improves the reconstruction efficiency of tracks emerging from secondary vertices which are significantly displaced from the *pp* collision position. This dedicated setup has empowered searches for long-lived particles in models beyond the Standard Model, extending their sensitivity to a larger lifetime range, and its performance is documented in this note.

ATL-PHYS-PUB-2017-014
24 July 2017

1 Introduction

Theories beyond the Standard Model (BSM) often predict the existence of new particles with relatively long lifetimes such that they can travel a significant distance through the ATLAS detector before decaying [1–6]. When the lifetime is of $O(0.1)$ to $O(10)$ ns, the decay has a sizable probability to take place within the ATLAS inner detector (ID). Searches for such particles have been performed by the ATLAS Collaboration in the past [7–9], reconstructing explicitly these decay vertices within the ATLAS inner detector volume.

The standard reconstruction of the trajectories of charged particles, referred to as tracks, in the ATLAS [10] inner detector is optimized for particles that point back to the primary pp interaction (IP), which are referred to as primary particles (dedicated algorithms are used to reconstruct some specific topologies of displaced decays, such as from photon conversions and $b-$hadron decays, but they are limited to these topologies and target particles with moderate impact parameters). Stringent requirements are placed on the transverse and the longitudinal impact parameters of the reconstructed candidate tracks relative to the primary vertex to keep the computation time reasonable while still being very efficient in reconstructing primary particles with high purity. This setup is not optimal for BSM searches that aim to detect decay products of particles whose decay vertex is significantly displaced from the IP, especially for transverse displacements greater than approximately 20 mm.

The analysis strategy for these searches entails selecting a subset of the recorded events based on the output of the standard reconstruction for special processing. In this processing, a dedicated track reconstruction algorithm, referred to as large radius tracking in the rest of this note, is run to improve the reconstruction efficiency for particles originating from such displaced decays at the cost of a longer computational time. This strategy is affordable since it is only applied to $O(1\%)$ fraction of the events recorded by the ATLAS detector.

This note describes the performance of this dedicated track reconstruction. Section 2 contains an overview of the ATLAS ID, Section 3 lists the Monte Carlo (MC) simulation and data samples used to estimate the performance. The details of the track reconstruction algorithms are outlined in Section 4. Section 5 presents a comparison between large radius tracking performance on data and MC simulation minimum-bias samples. Detailed results based solely on simulation are presented in Section 6: efficiency, resolution, track quality, and robustness against pileup are discussed in this section. This note does not, however, address the performance of the vertexing algorithms often used in these searches to reconstruct the decay vertices from these tracks.

2 ATLAS inner detector

The ATLAS inner detector [10] is cylindrical with forward-backward symmetry[1]. It is composed of a silicon pixel detector with four layers in the barrel, and three endcap disks on each side; and silicon microstrip (SCT) detectors with four layers in the barrel and nine endcap disks on each side. A transition radiation tracker (TRT) provides improved momentum measurement in the region $|\eta| < 2.0$. When

[1] ATLAS uses a right-handed coordinate system with its origin at the nominal interaction point in the center of the detector and the z-axis along the beam pipe. The x-axis points from the nominal interaction point to the center of the LHC ring, and the y-axis points upwards. Cylindrical coordinates (r, ϕ) are used in the transverse plane, ϕ being the azimuthal angle around the z-axis. The pseudorapidity is defined in terms of the polar angle θ as $|\eta| = -\ln\tan(\theta/2)$. Angular distance is measured in units of $\Delta R \equiv \sqrt{(\Delta\eta)^2 + (\Delta\phi)^2}$.

combined, the silicon detectors cover a range of $\eta < 2.5$, extend to a radius of 549 mm and $|z| < 805$ mm in the barrel, and a radius of 610 mm and $|z| < 2797$ mm in the endcap, as seen in Figure 1.

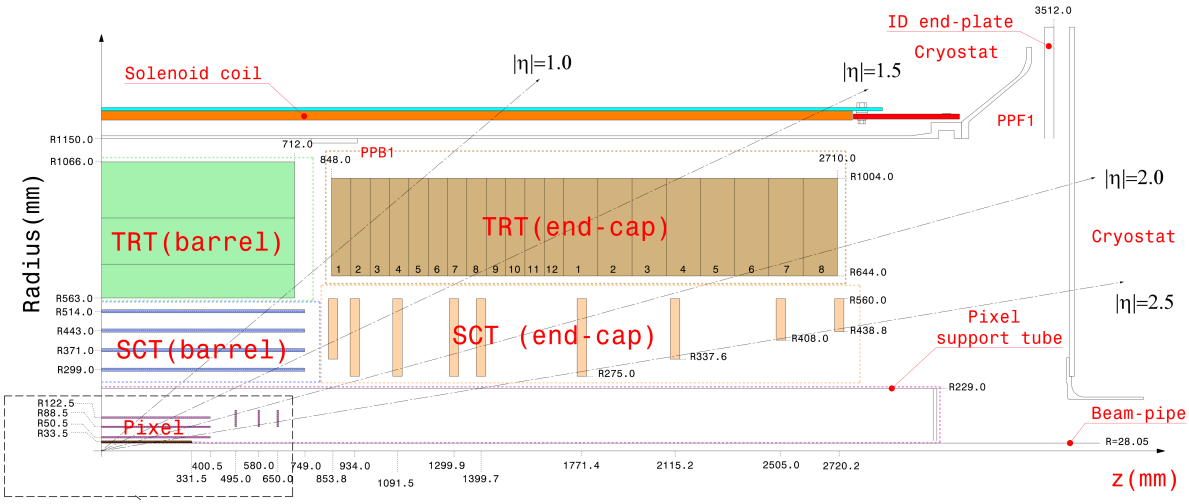

Figure 1: Schematic view of the inner detector layout.

The TRT has a radius from 554 to 1082 mm and $|z| < 780$ mm in the barrel, and a radius 617 to 1106 mm and $827 < |z| < 2744$ mm in the endcap. Due to its straw tube structure, the TRT barrel measures only the r and ϕ coordinates, and the endcap only z and ϕ, where each measurement has an intrinsic resolution of 120 µm. The advantage of the TRT is that there are over 52 000 straw tubes in the barrel which are 1.5 m long and run parallel to the beam axis, and over 120 000 tubes which are 0.4 m long and arranged radially in each endcap. These allow the TRT to add an average of about 30 two-dimensional additional points to reconstructed tracks that have $|\eta| < 2.0$.

Minimum-bias trigger scintillators (MBTS) are mounted at each end of the detector in front of the liquid-argon end-cap calorimeter cryostats at $z = \pm 3.56$ m and segmented into two rings in pseudorapidity ($2.07 < |\eta| < 2.76$ and $2.76 < |\eta| < 3.86$). They provide an efficient trigger with minimum bias for pp collisions used for a subset of the studies presented in this note.

3 Simulation and data samples

A comparison between the performance of the large radius tracking in data and in MC simulation has been done with a subset of data recorded at low instantaneous luminosity, corresponding to an average number of interactions per bunch crossing (pileup, or $\langle\mu\rangle$) of about 0.6. The data was collected using a minimum-bias trigger that requires at least one hit in each MBTS scintillator [11]. About 1.4 million events were processed, corresponding to roughly 12.6 nb^{-1} of integrated luminosity. The data is compared with a simulation sample generated using Pythia 8.186 [12]. The ATLAS minimum-bias tune `A2` [13] is used, which is based on the `MSTW2008LO` PDF [14].

Two sets of BSM physics processes have also been used to estimate the performance of the large radius tracking. Both of these samples are based on supersymmetry (SUSY) models which have long-lived particles (LLP) that decay at significantly displaced radial position $r \equiv x^2 + y^2$ in the ATLAS detector, but which are primarily in the central η region, and thus have a high probability of decaying within the

geometric acceptance of the inner detector. These BSM physics benchmark models provide the basis for a fair assessment of the large radius tracking.

The first of these two samples is squark pair production, with each squark decaying to a quark and the lightest neutralino ($\tilde{\chi}_1^0$). In this model, the $\tilde{\chi}_1^0$ subsequently decays through an R-parity violating (RPV) coupling to final states of pairs of displaced leptons, ee, $e\mu$, and $\mu\mu$, plus a neutrino (see Figure 2(a)). However in the present note only muons (from the $e\mu$ and $\mu\mu$ states) are considered. The mass of the squark is set to 700 GeV, the $\tilde{\chi}_1^0$ mass is set to 500 GeV and the lifetime of the $\tilde{\chi}_1^0$ is set such that $c\tau$ = 30 mm; the resulting transverse momentum (p_{T}) spectrum of the final state muons from the neutralino decay is quite hard, peaking at $p_{\mathrm{T}} \sim 100$ GeV. At most two tracks are produced from each neutralino decay. Such a scenario provides a relatively central signature well suited to test the ATLAS inner detector performance. This sample will henceforth be referred to as *displaced leptons*.

The second process used in these studies is predicted by Split SUSY theories [2], where pair-produced gluinos are long-lived due to the requirement of a decay to a heavy virtual squark ($O(> 1\mathrm{TeV})$), and can hadronize with ordinary partons creating R-hadrons. The pair-produced gluinos will hadronize into the R-hadrons, bound states with a color-charged supersymmetric particle and SM quarks, before decaying to a quark, and a squark which in turn decays to a quark and a neutralino, as shown in Figure 2(b), producing displaced hadronic jets in the inner detector. The mass of the gluino is set to 1.4 TeV and the mass of the neutralino is set to 1.3 TeV, which result in a relatively soft p_{T} spectrum for the hadronic decay products on the order of few GeV, with tails up to few tens of GeV. Many tracks are produced from each of the squark decays. This second sample will be referred to as *displaced hadrons*, due to the hadronic nature of the decay products.

In this note, leptons and hadrons produced in the decay of the long-lived particles, neutralinos in displaced leptons sample and gluinos in displaced hadrons sample, will be referred to as *signal particles*.

Figure 3 shows the transverse impact parameter d_0 for all truth particles (particles generated in the MC simulation), and signal truth particles, as well as the production radius (r_{prod}) and p_{T} for the signal particles in both of the two benchmark samples considered. The two benchmark samples have been chosen to show complementary lifetime, p_{T} spectrum, and hadron versus lepton composition.

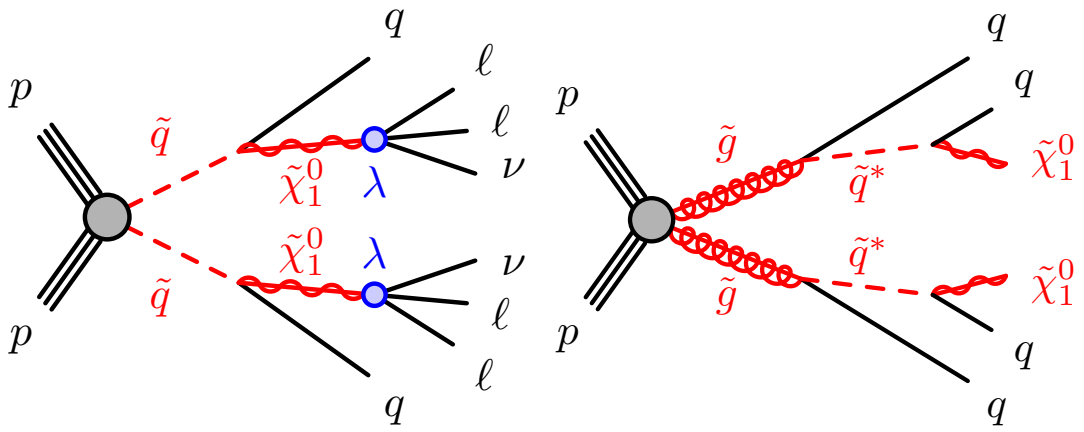

(a) Production of squarks decaying via long-lived neutralinos in R-parity violating SUSY

(b) Production of long-lived gluino pairs in Split-SUSY

Figure 2: Representative Feynman diagrams of the two samples used for the studies presented in this note.

The displaced hadrons sample was simulated using PYTHIA 6.428 [15]. The AUET2B [13] set of tune parameters for the underlying event and the CTEQ6L1 [16] parton distribution function (PDF) set are used. Dedicated PYTHIA routines [17–19] for hadronization of heavy colored particles are used to model the production and hadronization of the gluinos. The produced R-hadron is then propagated through ATLAS using GEANT4 [20] and its decay to quarks and neutralinos is handled by Pythia [21]. The displaced leptons sample was generated with MG5_aMC@NLO [22] interfaced to PYTHIA 8.186 [12] parton shower model.

The number of events generated is ten thousand for both samples. The response of the detector is simulated for both samples using a GEANT4 [20] framework.

The signal samples were overlaid with simulated minimum-bias events to model pileup. The distribution of $\langle\mu\rangle$ ranges approximately between 10 and 40, with a distribution that matches what is observed in the 2015 and 2016 pp data.

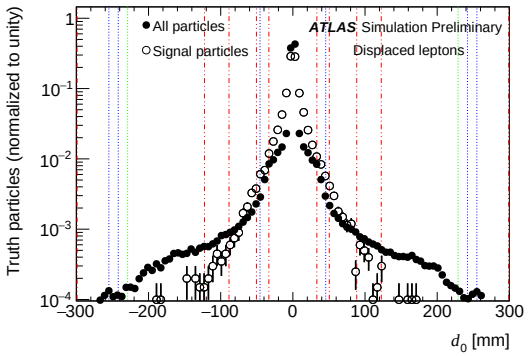

(a) True impact parameter d_0 for all truth particles and for muons from the LLP decays

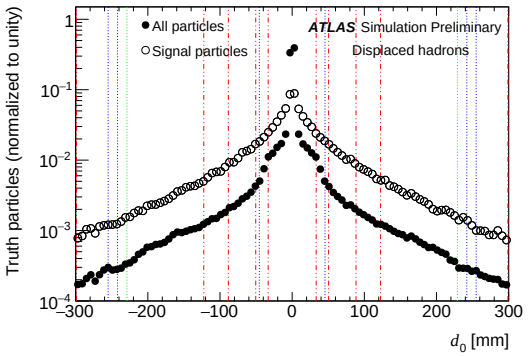

(b) True impact parameter d_0 for all truth particles and for hadrons from the LLP decays

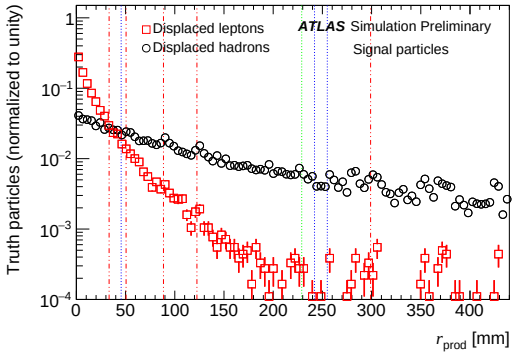

(c) True r_{prod} for signal particles of both samples

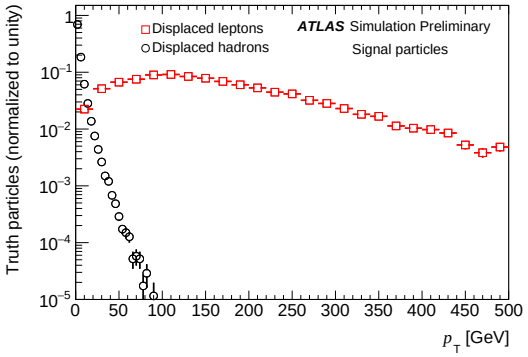

(d) Truth p_{T} for signal particles of both samples

Figure 3: Transverse impact parameter, d_0, for all truth particles and truth particles produced in the decay of the long-lived particle in the displaced leptons (a) and displaced hadrons (b) samples, normalized to unity. The blue dotted lines represent the inner and outer limits of the sub-detector envelopes (pixel and SCT), and the red dashed lines represent the detector layers from the first pixel layer at 33.25 mm to the first layer of the SCT at 299 mm. The green dotted line represents the end of pixel support tube. The production radius (c) and the p_{T} spectrum (d) for the signal truth particles for both samples are shown to demonstrate the complementary nature of the chosen signal samples.

4 Track reconstruction

4.1 Standard tracking

Track reconstruction in the inner detector primarily uses an *inside-out* track finding strategy, followed by an *outside-in* tracking. The track reconstruction algorithm first looks for a track seed in the pixel and SCT detectors, which is a collection of three space points[2] each from a unique layer of the pixel or SCT detectors. Track seeds can be built from three pixel space points, three SCT space points, or a combination of space points from both detectors. If the track seed passes certain quality criteria, including a p_{T} and impact parameter selection, a window search is constructed from the track seed and track candidates are formed using a combinatorial Kalman filter. A more detailed description of the silicon pattern recognition algorithm can be found in Ref. [23].

Track candidates are then processed by the so-called ambiguity-solving algorithms. Track candidates are evaluated based on various requirements including momentum, number of hits, number of shared modules, and holes[3]. Further details on the ambiguity solving stage are given in Refs. [23, 24].

The extension of tracks seeded in the silicon detectors, into the outer TRT detector, is performed by a classical track extrapolation where TRT hits compatible with the extrapolation are assigned to the track candidate. The quality of the resulting extension is evaluated based on the track fit and a track score calculated using tools similar to those used in the ambiguity solving. Any track which is successfully extended from the silicon detectors into the TRT is said to have a *TRT extension*.

If a track cannot be extended, the extension is marked as *failed*, but the track is still retained, a track may not be be extended into the TRT at large $|\eta|$. If a track is extended, but this extended track receives a worse score than the non-extended track, the track is marked as *rejected* (these tracks are also retained in the final track collection). This can happen if there are too many TRT outliers (where the track passes outside the TRT straw tube or a TRT hit detrimentally impacts the χ^2 of the track candidate), or if more than 50% of the TRT hits are tube hits (TRT hits which have no leading edge or for which the track does not pass through the drift circle within the straw tube, see Figure 4); finally, one can have a successfully extended track when the track has TRT hits which improve the overall track fit.

A second tracking pass, referred to as *outside-in*, is then performed reconstructing standalone TRT track segments in regions seeded by the electromagnetic calorimeter. The resulting TRT segments may then be extended back into the silicon detectors by associating any hits not already used for existing tracks from the *inside-out* pass. This pass may recreate some tracks which originate far from the IP but still have small impact parameters. TRT segments without any silicon hit are also kept and used for tasks as photon conversion reconstruction.

The resulting tracks, from both inside-out and outside-in strategies, form the final collection of reconstructed standard tracks. Tracks are described by five parameters and a reference point, using a perigee representation. Two of the parameters are the transverse (longitudinal) impact parameter d_0 (z_0), defined as the point of closest approach of the track in the transverse (longitudinal) plane to the reference point.

[2] A space point is defined as a measurement in the pixel detector or the combination of axial and stereo layers of the SCT detectors.

[3] Hits are defined as measurements from the Pixel, SCT, or TRT detectors; a hole is defined as a missing hit on an active module where one was expected based on the particle trajectory; only silicon detectors are considered in the calculation of holes. Modules are the individual silicon sensors. A shared pixel module has at least one shared pixel hit and an SCT module is shared if it has at least two shared SCT hits.

The other three parameters are the azimuthal angle ϕ and the polar angle θ of the track momentum at the reference point and the ratio q/p of the charge of the reconstructed track divided by the magnitude of its momentum. The reference point used is the average position of the pp interactions (beamspot position) [25]. In the following note, the longitudinal impact parameter z_0 is however evaluated as the distance of the point of closest approach of the track to the beamspot position and the position of the primary pp collision vertex (the hard-scattering vertex).

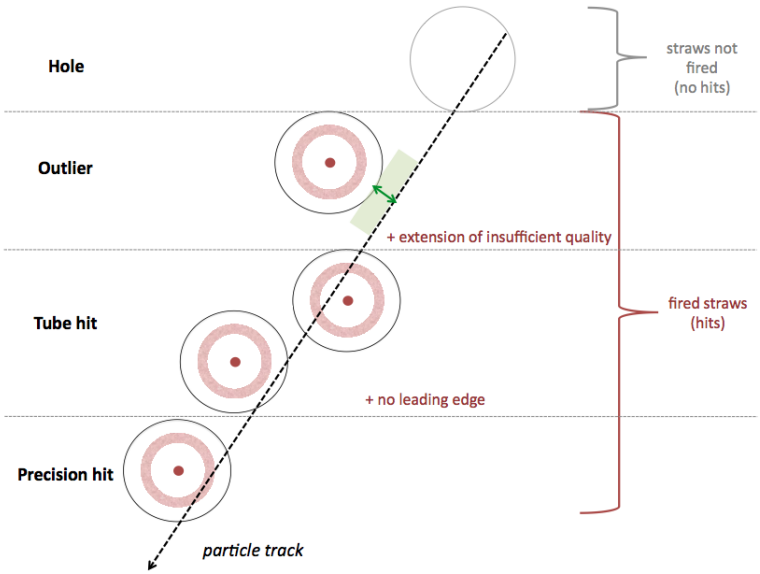

Figure 4: Definition of TRT hits. Precision hit: a hit with a residual within ± 2.5 standard deviations of the hit resolution. Tube hit: a hit inside the straw wall but not precise, i.e. it has a measured residual outside ± 2.5 standard deviations of the hit resolution or a hit on track with no valid leading edge. Outlier: a hit on track for which the fitted track passes 100 µm or more outside of the straw wall. Holes: straws crossed by a fitted track but with no hit.

4.2 Large radius tracking

The large radius tracking can be performed as a third tracking sequence, following the standard *inside-out* and *outside-in* tracking. It follows the same reconstruction strategy as the standard *inside-out* tracking but with relaxed selections on track impact parameters and number of hits, the most important of which are listed in Table 1. The large radius tracking allows the reconstruction of tracks originating in the inner detector far from the IP as opposed to the standard track reconstruction, optimized for finding tracks pointing back to the IP.

This extra reconstruction sequence is not applied in the standard ATLAS reconstruction, but it is applied only to approximately a few percent of the data samples used for physics analysis, which are selected based on event-level quantities computed during the standard reconstruction. Such pre-selection allows for the separate storage of the unprocessed data events for further processing. Given that these data events are processed separately, the requirements on the computational resources available for this extra processing step are less stringent with respect to the standard ATLAS reconstruction.

In the track seeding and track candidate creation stage, space points are created from un-used hits, which are silicon hits that have not been used in the standard *inside-out* and *outside-in* tracking. The pattern

	Standard	Large radius
Maximum d_0 (mm)	10	300
Maximum z_0 (mm)	250	1500
Maximum $\|\eta\|$	2.7	5
Maximum shared silicon modules	1	2
Minimum unshared silicon hits	6	5
Minimum silicon hits	7	7
Seed extension	Combinatorial	Sequential

Table 1: Most important selections that differ between the standard and the large radius tracking setups.

recognition algorithm uses these space points to create track seeds, and a window search is applied in the seed direction to build track candidates, with relaxed tracking parameter requirements as stated above. The strategy used to extend seeds into track candidates is also different from the standard reconstruction and prevents the creation of multiple track candidates from the different possible combinations of points by using a sequential Kalman filter approach, instead of using a combinatorial Kalman filter.

The same relaxed impact parameter selections are imposed in ambiguity solving as the selections in the track seed creation. The maximum number of shared hits (hits considered in more than one reconstructed track fit) and minimum number of not-shared hits are also loosened to retain high reconstruction efficiency.

Tracks accepted by the ambiguity solver are extended to the TRT. The same set of selections (impact parameters, $|\eta|$, hit requirements) used in the preceding steps are implemented here for consistency. The resulting collection of tracks, whether they have a valid TRT extension or not, is merged into the standard track collection and form the final track collection.

The time needed to run the complete ATLAS event reconstruction including large radius tracking increases by about a factor of 2.5 with respect to the standard configuration, when running on a sample with similar pileup distribution as observed in 2015 and 2016 data.

4.3 Fiducial selections

In order to study the performance of the tracking on MC simulation, a hit-based matching scheme is adopted, where tracks matched to truth particles with a matching probability (p_{match}) above a certain threshold are classified as *well-reconstructed*. Each hit is associated to a truth particle and such probability is calculated based on the particle that contributes the most to the reconstructed track. To assess the feasibility of using this matching scheme, and which probability threshold to use for large radius tracks, Figure 5 shows the distribution of residuals of d_0 for the reconstructed tracks relative to their associated truth particle, in bins of matching probability and separately for standard and large radius tracks.

A degradation of the residuals with decreasing p_{match} is seen for both classes of tracks, while in both cases a threshold of 50% guarantees that the reconstructed track parameters are well correlated to the associated truth particle. A threshold of 50% in p_{match} is therefore applied in the following simulation studies for both standard and large radius tracks when matching to a truth particle.

In order to study the performance of reconstructing displaced particles, a set of fiducial selections are applied to the truth particles considered. Particles are required to have $p_{\text{T}} > 1$ GeV, $|\eta| < 2.5$, be

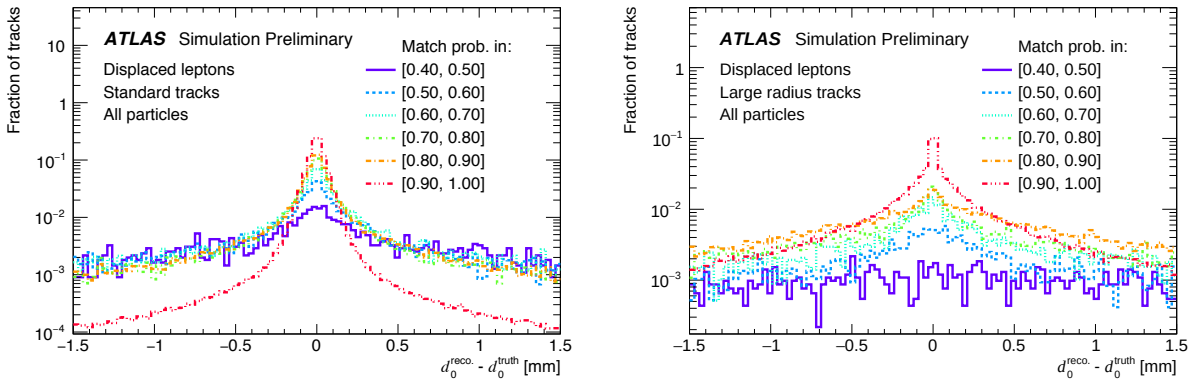

(a) Standard tracks

(b) Large radius tracks

Figure 5: Distributions of d_0 residuals for inclusive (a) standard and (b) large radius tracks in bins of the matching probability of the track for the displaced leptons sample.

electrically charged, and have $r_{\text{prod}} < 440$ mm to ensure that the decays of the LLPs are early enough such that the resulting tracks cross multiple layers in the SCT barrel. Truth particles considered to be signal are also required to be in the decay chain from the long-lived particle – the R-hadron or the neutralino. A summary of the fiducial selections is shown in Table 2.

p_{T}	$>$	1 GeV
$\lvert\eta\rvert$	$<$	2.5
r_{prod}	$<$	440 mm
charge	$=$	± 1
From LLP decay (signal)		

Table 2: Fiducial selections applied to truth particles.

5 Data and simulation comparison

A basic comparison of the properties of reconstructed tracks by the large radius tracking between data and simulation is performed using a minimum bias sample, described in Section 3. The main source of non-prompt particles in this sample comes from hadrons produced in hadronic interactions of prompt particles with the material of the ATLAS detector, and they provide a basic test of the description of the quality of the reconstructed tracks for non-prompt particles.

Tracks are selected on those events in which at least one reconstructed primary vertex is present and there is at least one track in the event fulfilling basic quality requirements as described in Ref. [26]. The events in the simulation are weighted in order to match the observed z distribution of interactions, and an event-wise weight is applied to the number of tracks per event, in addition to kinematic, p_{T} and η, weights in order to match the observed track distributions.

Figure 6 shows the distribution of the number of hits on track in data compared with simulation, and in Figure 7, the same observables are averaged for all tracks at the same η. In both cases, all reconstructed

tracks from both the standard as well as the large radius tracking are shown. The distributions in the simulation closely match the distributions in data. Small discrepancies are consistent with those shown in Ref. [11].

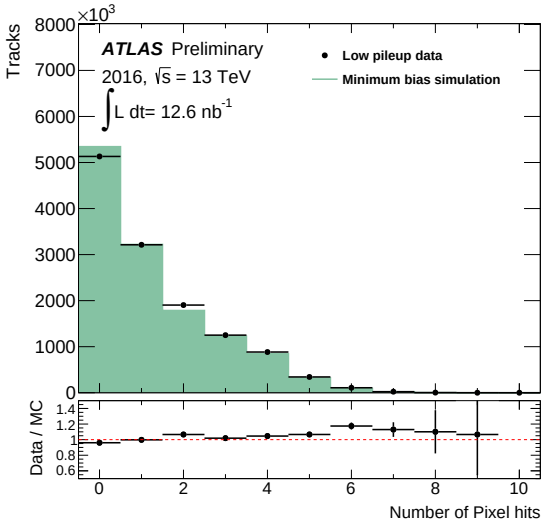

(a) Pixel hits

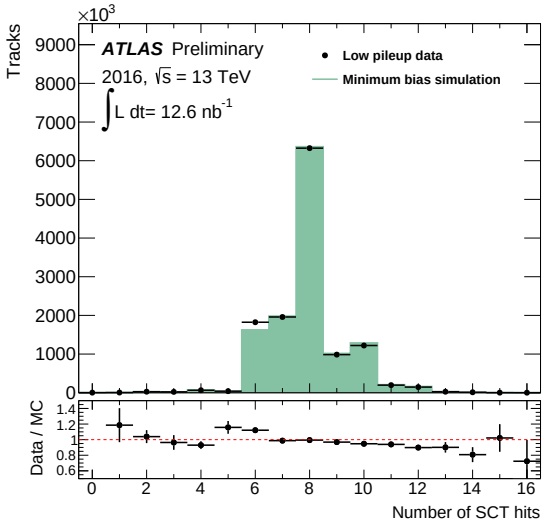

(b) SCT hits

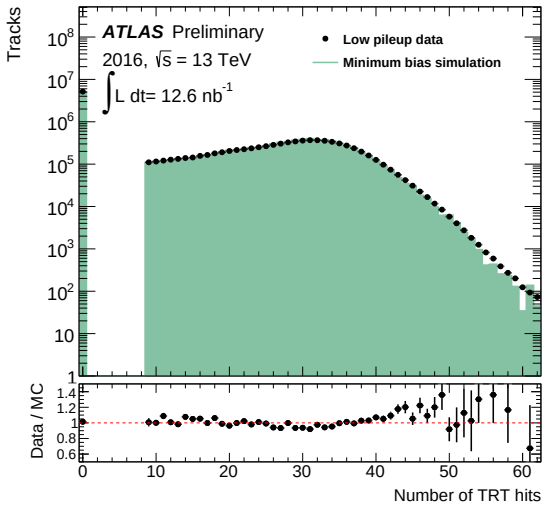

(c) TRT hits

Figure 6: Distributions of the number of hits in the pixel, SCT, and TRT detectors for data compared with simulation. Dead pixel and SCT sensors are included. Tracks with zero TRT hits represent tracks with no TRT extension. The simulation is normalized to the number of tracks in data. The uncertainty shown in the ratio plot represents the combined statistical uncertainties on the simulation and the data.

The transverse and longitudinal track impact parameters are shown in Figure 8. The structure of the transverse impact parameter distribution reflects the two sequences of track reconstruction that have been

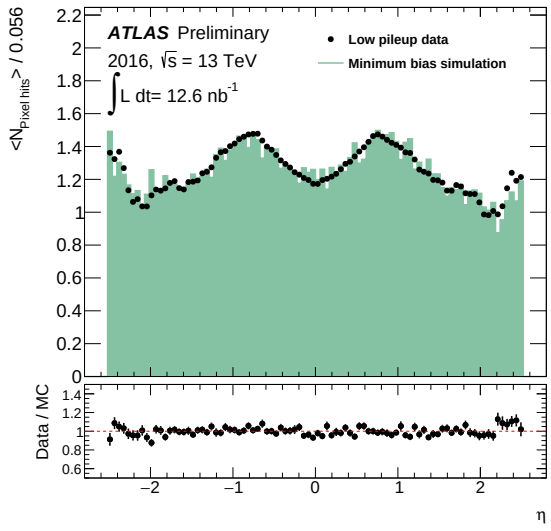

(a) Pixel hits

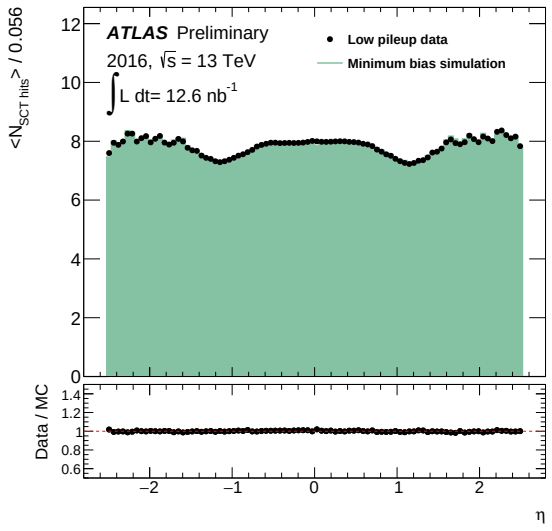

(b) SCT hits

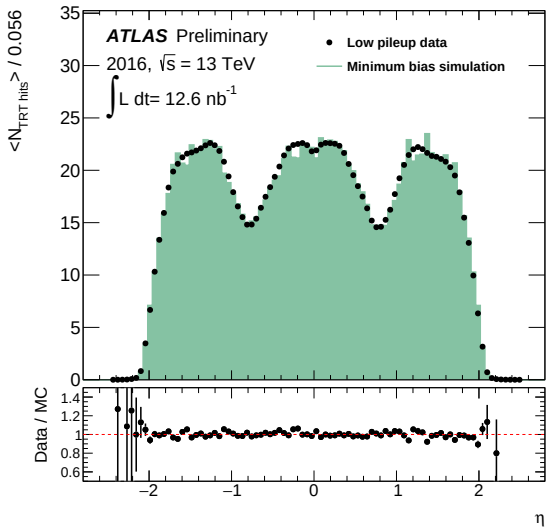

(c) TRT hits

Figure 7: Average number of pixel, SCT, and TRT hits as a function of the η of the track. Dead pixel and SCT sensors are included. The simulation is normalized to the number of tracks in data. The uncertainty shown in the ratio plot represents the combined statistical uncertainties on the simulation and the data.

run with different quality requirements (standard and large radius tracking). The central population is dominated by tracks reconstructed with the standard tracking algorithm, while the tracks populating the larger values of $|d_0|$ are primarily coming from the large radius tracking sequence. Similarly, for the longitudinal impact parameters the tracks reconstructed by the large radius tracking populate most of the tails of this distribution, although their contribution at smaller $|z_0|$ values (but high $|d_0|$) is also significant. In both cases, simulation reproduces well the distribution observed in data.

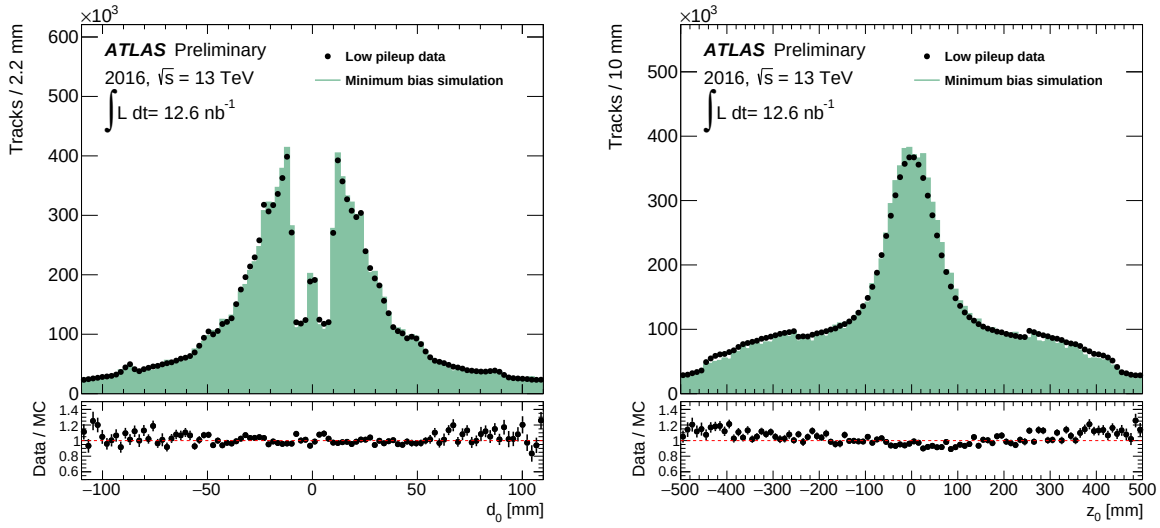

(a) d_0 (b) z_0

Figure 8: Transverse (a) and longitudinal (b) impact parameters in data and simulation. The simulation is normalized to the number of tracks in data. The uncertainty shown in the ratio plot represents the combined statistical uncertainties on the simulation and the data.

Figure 9 shows the distribution of the radius of the first measured hit on the track. Tracks reconstructed with the large radius tracking sequence significantly improve the ability of reconstructing non-prompt particles coming from hadronic interactions, which manifest as a population of tracks with radii of the first hit compatible with the detector material positions. Simulation does not perfectly reproduce the distribution observed in data, as a consequence of differences in the simulated and real detector geometry.

6 Performance studies on simulation

6.1 Reconstruction efficiency

To study the effect that large radius tracking has on the ability to reconstruct displaced particles, it is important to examine the efficiency for reconstructing the charged particles produced by BSM processes. In this note, the efficiency being referenced will always be the reconstruction efficiency, i.e. the ratio of

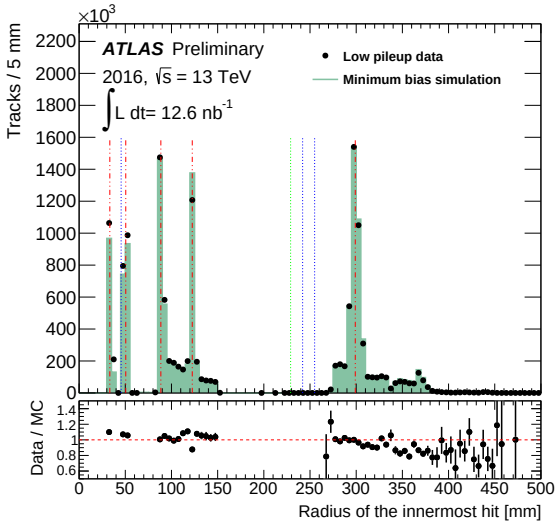

Figure 9: Distribution of the radius of the first measured hit in the tracks. The simulation is normalized to the number of tracks in data. The uncertainty shown in the ratio plot represents the combined statistical uncertainties on the simulation and the data. The blue dotted lines represent the inner and outer limits of the sub-detector envelopes (pixel and SCT), and the red dashed lines represent the detector layers from the first layer of the pixel detector at 33.25 mm to the first layer of the SCT at 299 mm. The green dotted line represents the end of the pixel support tube.

the number of tracks matched to a signal truth particle passing the fiducial requirements listed in Table 2 and the number of signal truth particles satisfying the same requirements:

$$\text{reconstruction efficiency} = \frac{\text{number of signal truth particles matched to reconstructed tracks}}{\text{number of signal truth particles}}. \quad (1)$$

For large radius tracking or standard tracking efficiency, the tracking requirement is applied exclusively to the numerator, and the combined efficiency takes into account all tracks in the final track collection.

The benchmark processes used are the ones listed in Section 3. The reconstruction efficiency, with the fiducial and the tracking parameter requirements listed in Section 4.3 imposed to the signal truth particles defined in Section 3, is shown in Figure 10 as a function of the production radius of the displaced particles.

The nature of the track reconstruction used by ATLAS is sequential, as described in Section 4, which results in the dependence of large radius tracking efficiency on r_{prod} shown in Figure 10; at low r_{prod} standard tracking is very efficient and few hits are left over to form tracks in the large radius tracking step. Tracks which are produced far from the interaction point are unlikely to be reconstructed by the standard tracking; without large radius tracking, fewer than 20% of the tracks with $r_{\text{prod}} > 50$ mm originating from the long-lived particle decay would be reconstructed, as is shown in Figure 10(b) in the case of the displaced hadrons sample (the fraction becomes about 30% from the displaced leptons sample, shown in Figure 10(a)). The addition of the large radius tracking step increases substantially the reconstruction efficiency beyond r_{prod} of 50 mm for both benchmark samples.

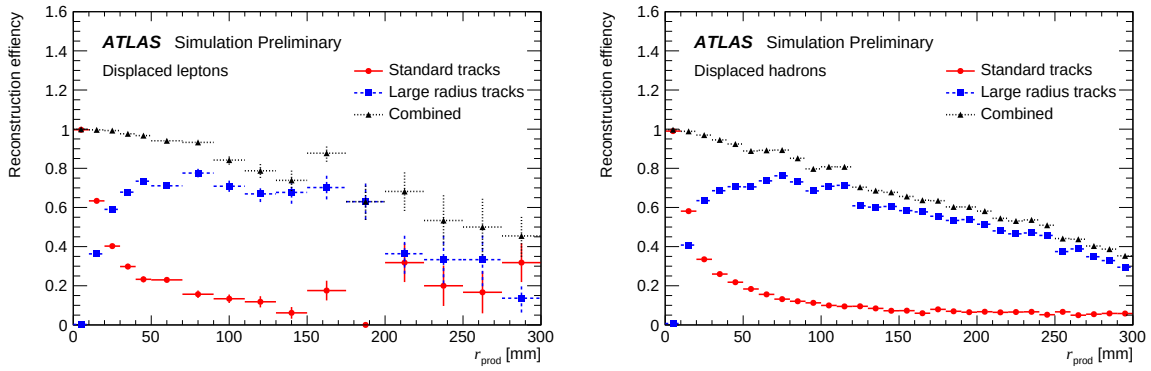

(a) Displaced leptons

(b) Displaced hadrons

Figure 10: Inclusive track reconstruction efficiency for displaced charged particles produced by the decay of long-lived signal particles. The efficiency is shown as a function of the radius of production of displaced particles (r_{prod}), with truth particles and tracks subject to fiducial selections. The efficiency for standard and large radius tracking is additive, and the total efficiency is the sum of both.

The efficiency shown in Figure 10 remains much below 100% for large r_{prod} even after the addition of the large radius tracking; this can arise in part from algorithmic inefficiencies as well as non-hermeticity of the detector for non-prompt particles or interactions of the particles with the ATLAS detector material. To separate these effects and to evaluate the algorithmic performance of the tracking setup, a so-called technical efficiency is defined. The technical efficiency is used to determine the reconstruction performance for truth particles that are expected to leave enough hits in the detector to be reconstructed by the tracking algorithms employed. To achieve this, requirements are placed on the number of energy deposits left by truth particles in the simulation samples on active elements of the silicon detectors, as well as basic acceptance selections. Such selections mimic the minimum requirements of track reconstruction. These are presented in Table 3, and are applied to the denominator in Eq. 1. The technical efficiency is an informative metric for understanding the performance of the large radius tracking as many particles which are produced far from the interaction point leave too few hits in the silicon to form a valid track and thus could not be reconstructed by any method using silicon track seeding.

Fiducial selections for technical efficiency		
r_{prod}	$<$	300 mm
$\lvert\eta\rvert$	$<$	5
p_{T}	$>$	1 GeV
Number of silicon hits	$\geq$	7

Table 3: Selections on truth particles used in the denominator of the technical efficiency. The minimum number of silicon hits refers to the number of energy deposits by the truth particle on active elements on the ATLAS silicon detectors.

As demonstrated in Figure 11(a), for the displaced leptons sample, the combined technical efficiency ranges between 90% to 100% for truth particles with r_{prod} extending past the last layer of the pixel barrel, and is still greater than 80% for those with r_{prod} out to 300 mm — the first layer of the SCT. Figure 11(b) shows the combined technical efficiency is slightly larger for the LLPs in the displaced hadrons sample, at least 90% across r_{prod} up to 300 mm. Figure 11 shows that for both types of samples, the large radius

tracking step is very efficiently reconstructing the tracks missed by standard tracking which cross the minimum number of silicon layers required for reconstruction.

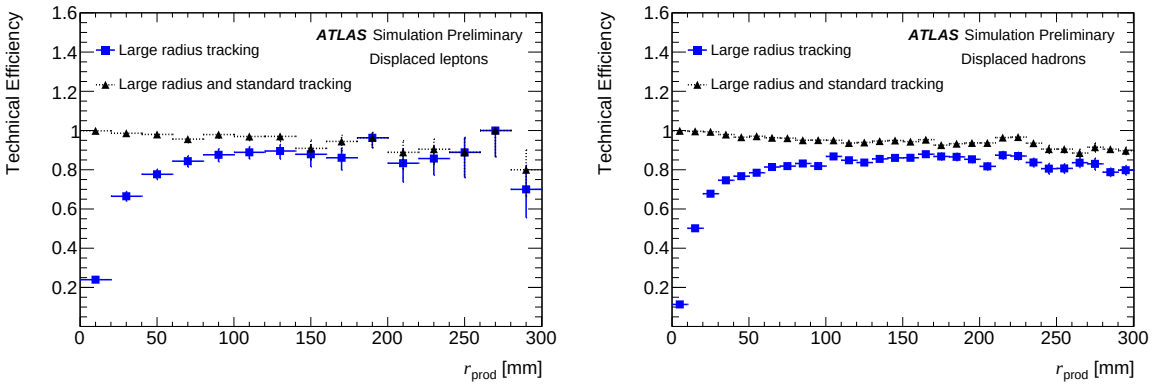

(a) Displaced leptons

(b) Displaced hadrons

Figure 11: Technical reconstruction efficiency of signal particles for large radius tracking and combined standard plus large radius tracking. The efficiency is shown as a function of r_{prod}.

6.2 Resolution

Section 6.1 shows that large radius tracking yields substantially increased efficiency for reconstructing charged signal particles, in particular at large production radii. However, in order for the reconstructed tracks to be useful for physics analyses, they must accurately represent the truth particles to which they are matched, ideally with a resolution comparable to that of standard tracking.

Figure 12 shows the residual of the d_0 parameter for standard and large radius tracks, measured as the difference of the reconstructed parameter of tracks relative to the signal particles in the MC truth record to which they are matched, for both displaced leptons and displaced hadrons signal samples. Similarly, Figure 13 shows the resolution of the q/p parameter.

Figures 12 and 13 show that, for both standard and large radius tracking, no bias is found in the measured parameters of tracks matched to signal particles. This is also true for the remaining track parameters. It is also seen that the widths of the residuals distributions for large radius tracks are somewhat larger than for standard tracks, which is to be expected: since large radius tracks are, on average, produced at larger radii from the interaction point than standard tracks (cf. Figure 3(c)), the extrapolation of the track parameters from the first hit on the track trajectory to the interaction point will naturally lead to larger uncertainties. Uncertainties on track parameters have also been studied using the distribution of residuals divided by the estimated uncertainty. For all track parameters the pull distributions are found to have a width consistent with unity, for both standard and large radius tracks.

From Figures 12 and 13, it is also seen that the resolution of the track parameters are significantly different for the two signal processes under consideration. However, this is as expected from a combination of the different lifetimes and p_{T} spectra, cf. Figures 3(c) and 3(d), and to a lesser extent decreased multiple scattering effects in the case of the lepton signature compared to the hadronic one, cf. Figure 3(c). The signal particles in the two processes have markedly different characteristic transverse momenta: whereas for the leptonic signature, the signal leptons are produced by resonance decay, cf. Figures 2(a), and

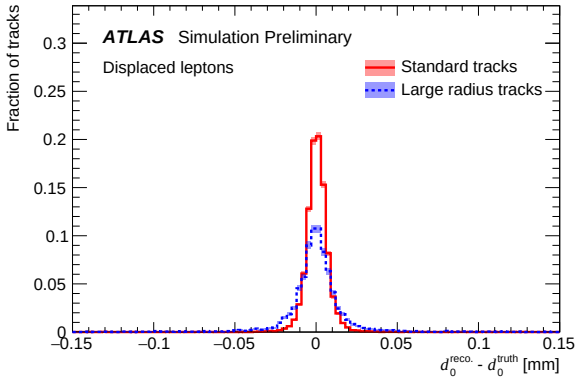

(a) Displaced leptons

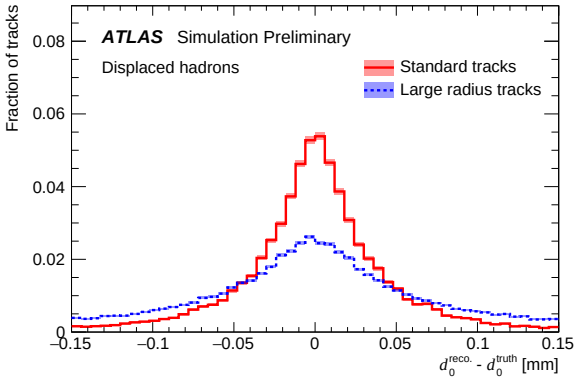

(b) Displaced hadrons

Figure 12: Normalized distributions of the difference between the transverse impact parameter, d_0, for the truth particle and the corresponding reconstructed track, for signal particles in the (a) displaced leptons and (b) displaced hadrons samples, comparing standard and large radius tracks.

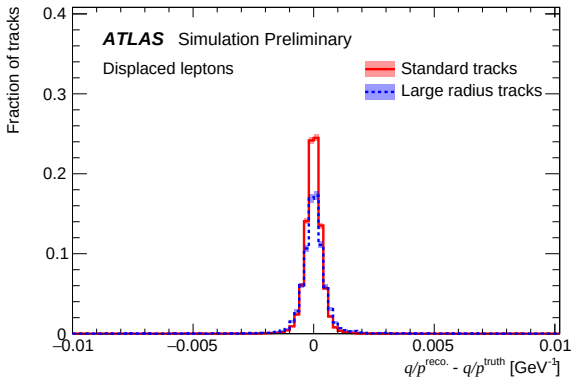

(a) Displaced leptons

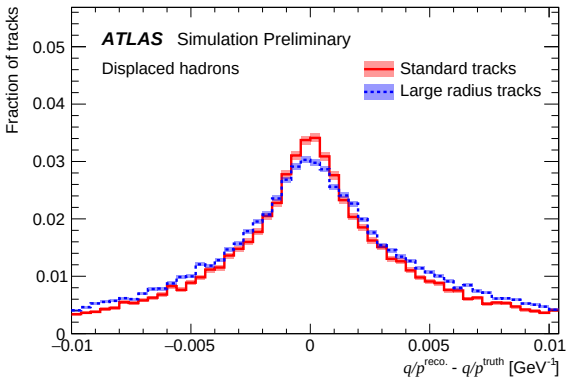

(b) Displaced hadrons

Figure 13: Normalized distributions of the difference between the charge over momentum, q/p, for the truth particle and the corresponding reconstructed track, for signal particles in the (a) displaced leptons and (b) displaced hadrons samples, comparing standard and large radius tracks.

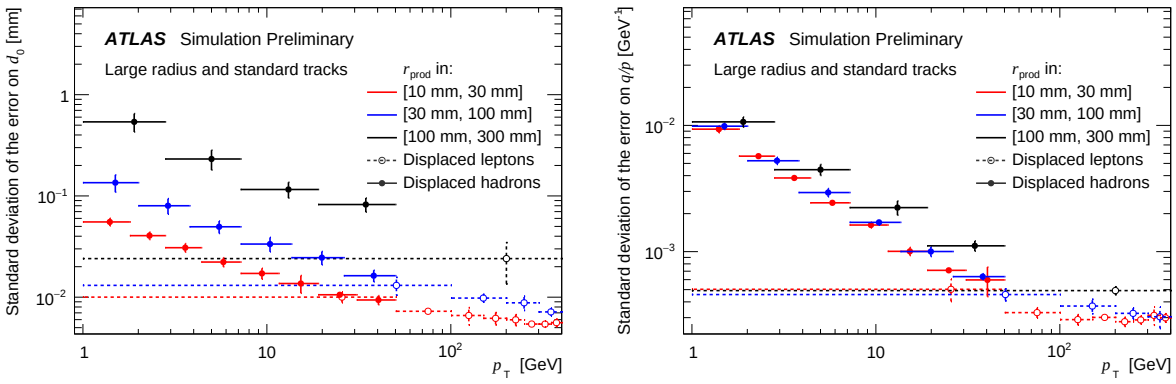

(a) Standard deviation of the error on d_0

(b) Standard deviation of the error on q/p

Figure 14: Standard deviations of the (a) d_0 and (b) q/p parameter residual distributions for combined standard and large radius signal tracks as function of the p_T of the associated truth signal particle from the displaced hadrons and displaced leptons samples.

thus have a peaking p_T spectrum with an average p_T of around 150 GeV, the signal particles in the hadronic signature are not, cf. Figure 2(b), yielding an exponential p_T spectrum with an average of around 5 GeV, leading to comparably worse parameter resolution (see Figure 3(d)). However, in both cases each reconstructed track parameter is an unbiased estimator of the corresponding parameter for the matched truth particle within estimated errors.

Figure 14 shows the resolution of track parameters, measured as the standard deviation of residual distributions similar to those in Figures 12 and 13, as a function of the track p_T for signal tracks in the displaced hadrons and leptons processes. The profiles are shown in bins of the truth particle production radius, r_{prod}, over a representative range.

For each bin defined in r_{prod} and p_T, the $\pm 3\sigma$ core standard deviation of the parameter residuals is found by iteratively fitting the corresponding distribution with a gaussian function and gradually increasing the range around the central peak on which the fit is performed, until this range covers ± 3 fitted standard deviations. This is done in order to limit the impact of spurious outliers on the parameter error profiles in Figures 14 and 17(a). The core standard deviation defined in this way, and the associated statistical uncertainty, are found as the corresponding fit parameter and its error. In addition, similar fits are performed to the core $\pm 2\sigma$ and $\pm 2.5\sigma$ ranges in the same way, and the largest absolute difference between the $\pm 3\sigma$ core standard deviation and either of the standard deviations found in the additional fits is added in quadrature to the statistical uncertainty as a measure of the ambiguity in the definition of the core of the residuals distribution.

As expected, the residual distribution, due to the non-gaussianity of the entire distribution, is seen to be better at smaller production radii and degrading with r_{prod}. In particular, it is seen that resolution deteriorates abruptly for tracks produced at the edge of, or outside, the ATLAS pixel detector, as would be expected considering the spatial resolution of hits in the pixel layers and their associated weight in the estimation of track parameters. It is also seen that the resolution improves with p_T, as expected, and is consistent between the displaced hadrons and leptons samples. This illustrates that the differences in resolution between the two samples, shown in Figures 12 and 13, do indeed arise as a consequence of differences in lifetime and p_T. The resolution profiles shown in Figure 14 are for the combined category of

tracks, i.e. for both standard and large radius tracks. This shows the overall expected resolution available to physics analyses using large radius tracks in addition to standard tracks, and is warranted since the profiles for standard and large radius tracks separately are in reasonable agreement within errors.

6.3 Track quality

A track is considered to be of poor quality if the matching probability, between the reconstructed track and the track created by the hits from a truth particle, is less than 50% (Section 4) or if the track is not matched to an identified truth particle. The number of such reconstructed tracks divided by the total number of reconstructed tracks is defined as *poor-quality track rate*.

Since large radius tracking is more susceptible to random-hit combinatorics, the poor-quality track rate is much higher for large radius tracking than it is for standard tracking. For both the displaced hadrons and displaced leptons samples processed, the rate of poor-quality tracks is nearly 80%.

It is considered more important to maximize the efficiency than to minimize the rate of poor-quality tracks; to reconstruct and retain as many true tracks as possible to prevent the information from being lost before focusing on reducing the poor-quality tracks. As the technical efficiency plots show (see Figure 11), the overall efficiency for reconstructing tracks that meet minimum requirements for number of hits, etc, is approximately 90% or above for $0 < r_{\text{prod}} < 300$ mm. Thus it is possible to take steps to reduce the number of poor-quality tracks.

The poor-quality track rate can be reduced by tightening the requirements on the number of TRT hits as well as on the number of SCT hits. The poor-quality track rate also shows significant correlation with the quality of the TRT extension, which can be measured in part by examining the TRT precision hit fraction. As seen in Figure 15(a), raising the minimum number of TRT hits for TRT extended tracks to 20 would cut out primarily poor-quality tracks while keeping the majority of the tracks matched to signal particles for the displaced hadrons sample. Similarly, Figure 15(b) demonstrates that the majority of tracks with a TRT precision hit fraction below 0.6 are poor quality, while the majority of signal matched tracks have a TRT precision hit fraction of greater than 0.6 and nearly all have a precision hit fraction greater than 0.5. Due to the fact that for future data collection, the minimum precision hit fraction required for a successful TRT extension will be set to 0.3 or less for standard tracking, the understanding and separate optimization of this parameter for large radius tracking is especially important. Plots are shown for the displaced hadrons sample, but results are very similar for the displaced lepton sample — the primary difference being the crest of the signal peak for the lepton sample begins at 0.75 for the TRT precision hit fraction rather than 0.7 for the hadron sample, and at approximately 34 TRT hits rather than 32.

Figure 16 demonstrates that the majority of the tracks which have seven or fewer hits in the SCT are poor-quality tracks, while for the displaced hadrons sample shown, as well as for the displaced leptons sample, the majority of signal matched tracks have eight or more SCT hits. Therefore, it should be possible to reduce the poor-quality track rate by putting a restriction on the minimum number of SCT hits in tracks with larger impact parameter. While there is a requirement of a minimum of seven silicon (pixel and SCT combined) hits for both standard and large radius tracking, there is no minimum requirement on the number of SCT hits alone. Tracks with large impact parameters, however, are likely to have fewer pixel hits than most standard tracks, and would thus benefit from an extra condition placed on the number of SCT hits.

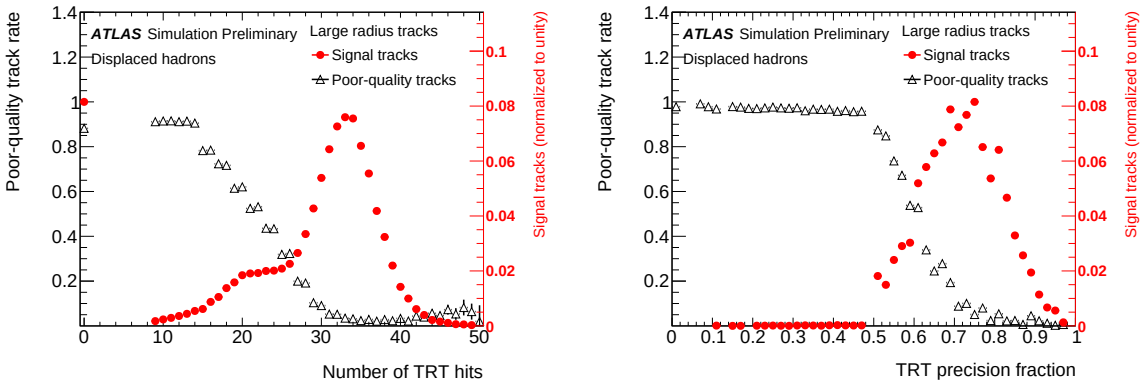

(a) Number of TRT hits

(b) TRT precision hit fraction

Figure 15: Summary plots for the rate of large radius tracks with poor quality contrasted with large radius tracks stemming from signal truth particles vs the number of TRT hits (a) and the TRT precision hit fraction (b). The signal-matched reconstructed tracks are normalized by the integral of the signal histograms. The last bin of (a) contains the overflow for all tracks with greater than 50 TRT hits.

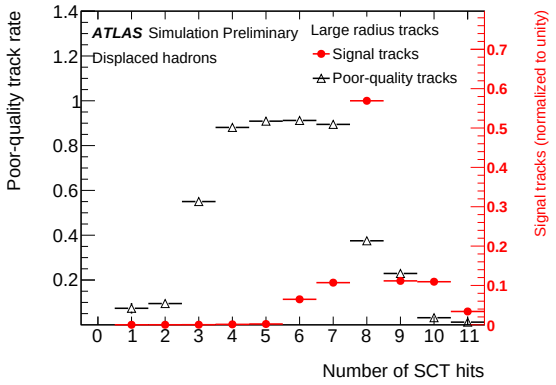

Figure 16: Summary plot for the rate of large radius tracks with poor quality, contrasted with large radius tracks stemming from signal truth particles vs the number of SCT hits per track. The signal-matched reconstructed tracks are normalized by the integral of the signal histogram. The last bin contains the overflow for all tracks with greater than 11 SCT hits.

In addition to the reduction in the poor-quality track rate that the above measures will provide, many of the remaining poor-quality tracks tracks will be eliminated by analyses during the vertexing step, and furthermore by the quality cuts placed on the vertices at the physics analysis stage.

6.4 Robustness against pileup

It is also necessary to assess the feasibility of utilizing large radius tracking in situations of high detector occupancy, considering the increasing amount of pileup expected during the LHC Run 2 and beyond. Therefore, the robustness, in terms of the stability with pileup levels, of track parameter resolution as well as inclusive reconstruction efficiency is shown in Figure 17.

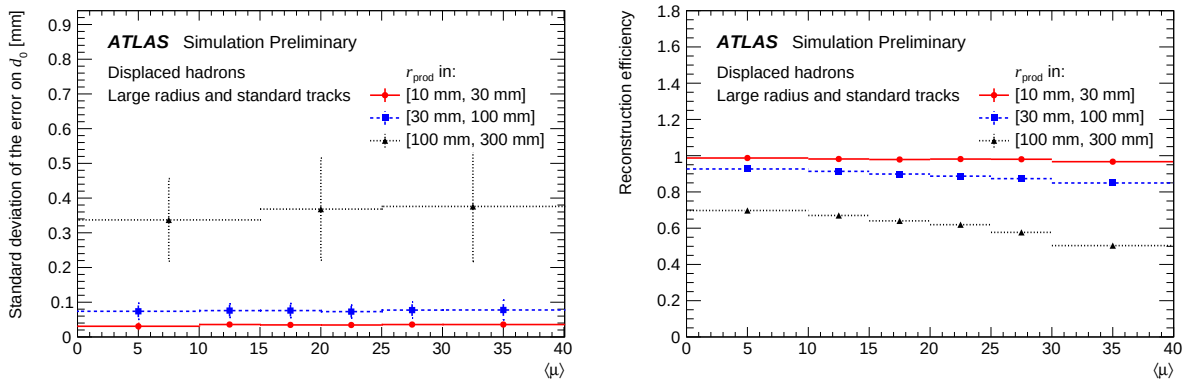

(a) d_0 resolution

(b) Inclusive reconstruction efficiency

Figure 17: Robustness of the (a) d_0 track parameter resolution and (b) inclusive reconstruction efficiency for standard and large radius tracks, as function of $\langle\mu\rangle$, in bins of the truth signal particle production radius in displaced hadrons events.

Figure 17(a) shows that the resolution of the d_0 track parameter does not show dependence on the pileup, up to $\langle\mu\rangle = 40$, for all production radii considered, which is also true for the remaining track parameters as well. Furthermore, both magnitude and stability of the track parameter resolution are compatible for both standard and large radius tracks. This indicates that the reconstruction of signal particles as large radius tracks is possible with good resolution even up to considerable pileup levels. The large uncertainties, in particular for the highest-r_{prod} bin, are driven by the ambiguity in the definition of the core standard deviation, since each bin in Figure 17(a) is inclusive in p_{T}. From Figures 14 it is seen that integrating over p_{T} leads to a distribution that does not contain a single well-defined notion of resolution, which the uncertainty accounts for. However, the stability of the observable in Figure 17(a) against $\langle\mu\rangle$ indicates that the underlying p_{T}-dependent d_0 resolution is not very sensitive to pileup.

Figure 17(b) shows the dependence of the reconstruction efficiency of signal particles as standard or large radius tracks. A significant fall-off with $\langle\mu\rangle$ can be seen, the effect increasing with r_{prod}. This behavior in the combined reconstruction efficiency is driven by a steady decrease in efficiency for large radius tracks, while standard tracking efficiency remains largely constant. This smaller fraction of signal particles being reconstructed with increased occupancy, as evidenced by Figure 17(b), is under investigation in order to ensure the retention of high reconstruction efficiency for large radius tracks in future LHC runs.

7 Conclusion

A dedicated tracking pass based on the standard tracking algorithms has been developed and used successfully for searches for new particles predicted in physics beyond the Standard Model which decay after traveling a significant distance inside the ATLAS inner detector. The description of the dedicated processing as well as its performance on benchmark physics processes has been presented.

The dedicated processing is found to be very efficient at reconstructing the decay products of such displaced decays whenever they happen within the pixel detector volume and out to the first layer of the SCT detector, as long as they deposit enough hits in the detector. In studies assessing the performance as a function

of pileup the resolution of the track parameters is found to be stable, but further work may significantly improve the reconstruction efficiency in the high-pileup environments expected in the rest of Run 2 and in Run 3.

References

[1] S. Dimopoulos, M. Dine, S. Raby, and S. D. Thomas,
Experimental signatures of low-energy gauge mediated supersymmetry breaking,
Phys. Rev. Lett. **76** (1996) 3494, arXiv: hep-ph/9601367 [hep-ph].

[2] N. Arkani-Hamed and S. Dimopoulos, *Supersymmetric unification without low energy supersymmetry and signatures for fine-tuning at the LHC*, JHEP **06** (2005) 073,
arXiv: hep-th/0405159 [hep-th].

[3] R. Barbier et al., *R-parity violating supersymmetry*, Phys. Rept. **420** (2005) 1,
arXiv: hep-ph/0406039 [hep-ph].

[4] M. J. Strassler and K. M. Zurek, *Echoes of a hidden valley at hadron colliders*,
Phys. Lett. **B651** (2007) 374, arXiv: hep-ph/0604261 [hep-ph].

[5] M. J. Strassler and K. M. Zurek, *Discovering the Higgs through highly-displaced vertices*,
Phys. Lett. **B661** (2008) 263, arXiv: hep-ph/0605193 [hep-ph].

[6] M. J. Strassler, *Possible effects of a hidden valley on supersymmetric phenomenology*, 2006,
arXiv: hep-ph/0607160 [hep-ph].

[7] ATLAS Collaboration, *Search for long-lived, massive particles in events with displaced vertices and missing transverse momentum in* $\sqrt{s} = 13$ *TeV pp collisions with the ATLAS detector*,
ATLAS-CONF-2017-026, 2017, URL: https://cds.cern.ch/record/2258161.

[8] ATLAS Collaboration, *Search for massive, long-lived particles using multitrack displaced vertices or displaced lepton pairs in pp collisions at* $\sqrt{s} = 8$ *TeV with the ATLAS detector*,
Phys. Rev. D **92** (2015) 072004, arXiv: 1504.05162 [hep-ex].

[9] ATLAS Collaboration, *Search for long-lived, weakly interacting particles that decay to displaced hadronic jets in proton–proton collisions at* $\sqrt{s} = 8$ *TeV with the ATLAS detector*,
Phys. Rev. D **92** (2015) 012010, arXiv: 1504.03634 [hep-ex].

[10] ATLAS Collaboration, *The ATLAS Experiment at the CERN Large Hadron Collider*,
JINST **3** (2008) S08003.

[11] ATLAS Collaboration, *Charged-particle distributions in* $\sqrt{s} = 13$ *TeV pp interactions measured with the ATLAS detector at the LHC*, Phys. Lett. B **758** (2016) 67, arXiv: 1602.01633 [hep-ex].

[12] T. Sjöstrand, S. Mrenna, and P. Z. Skands, *A Brief Introduction to PYTHIA 8.1*,
Comput. Phys. Commun. **178** (2008) 852, arXiv: 0710.3820 [hep-ph].

[13] ATLAS Collaboration, *Further ATLAS tunes of Pythia 6 and Pythia 8*,
ATL-PHYS-PUB-2011-014, 2011, URL: https://cds.cern.ch/record/1400677.

[14] A. Sherstnev and R. S. Thorne, *Parton Distributions for LO Generators*,
Eur. Phys. J. C **55** (2008) 553, arXiv: 0711.2473 [hep-ph].

[15] T. Sjöstrand, S. Mrenna, and P. Z. Skands, *PYTHIA 6.4 Physics and Manual*, JHEP **10** (2006),
arXiv: hep-ph/0603175.

[16] J. Pumplin et al.,
New generation of parton distributions with uncertainties from global QCD analysis,
JHEP **07** (2002) 012, arXiv: hep-ph/0201195 [hep-ph].

[17] M. Fairbairn et al., *Stable massive particles at colliders*, Phys. Rept. **438** (2007) 1,
arXiv: hep-ph/0611040 [hep-ph].

[18] G. R. Farrar and P. Fayet, *Phenomenology of the Production, Decay, and Detection of New Hadronic States Associated with Supersymmetry*, Phys. Lett. **76B** (1978) 575.

[19] A. C. Kraan, *Interactions of heavy stable hadronizing particles*, Eur. Phys. J. **C37** (2004) 91, arXiv: hep-ex/0404001 [hep-ex].

[20] S. Agostinelli et al., *GEANT4: A Simulation toolkit*, Nucl. instrum. Meth. A **506** (2003) 250.

[21] ATLAS Collaboration, *Search for long-lived stopped R-hadrons decaying out of time with pp collisions using the ATLAS detector*, Phys. Rev. D **88** (2013) 112003, arXiv: 1310.6584 [hep-ex].

[22] J. Alwall et al., *The automated computation of tree-level and next-to-leading order differential cross sections, and their matching to parton shower simulations*, JHEP **1407** (2014) 079, arXiv: 1405.0301 [hep-ph].

[23] ATLAS Collaboration, *Performance of the ATLAS Silicon Pattern Recognition Algorithm in Data and Simulation at* $\sqrt{s} = 7$ *TeV*, ATLAS-CONF-2010-072, 2010, URL: https://cds.cern.ch/record/1281363.

[24] ATLAS Collaboration, *The Optimization of ATLAS Track Reconstruction in Dense Environments*, ATL-PHYS-PUB-2015-006, 2015, URL: https://cds.cern.ch/record/2002609.

[25] ATLAS Collaboration, *Reconstruction of primary vertices at the ATLAS experiment in Run 1 proton–proton collisions at the LHC*, (2016), arXiv: 1611.10235 [hep-ex].

[26] ATLAS Collaboration, *Track Reconstruction Performance of the ATLAS Inner Detector at* $\sqrt{s} = 13$ *TeV*, ATL-PHYS-PUB-2015-018, 2015, URL: https://cds.cern.ch/record/2037683.